Ultrafast Science
A SCIENCE PARTNER JOURNAL

RESEARCH ARTICLE

Ultrafast Two-Electron Orbital Swap in Li Initiated by Attosecond Pulses

Hui Jiang[1], Zhao-Han Zhang[1], Yang Li[1], Camilo Ruiz[2], and Feng He[1,3*]

[1]Key Laboratory for Laser Plasmas (Ministry of Education) and School of Physics and Astronomy, Collaborative Innovation Center for IFSA (CICIFSA), Shanghai Jiao Tong University, Shanghai 200240, China. [2]Instituto Universitario de Física Fundamental y Matemáticas, Universidad de Salamanca, Plaza de la Merced s/n, 37008 Salamanca, Spain. [3]CAS Center for Excellence in Ultra-intense Laser Science, Shanghai 201800, China.

*Address correspondence to: fhe@sjtu.edu.cn

Citation: Jiang H, Zhang ZH, Li Y, Ruiz C, He F. Ultrafast Two-Electron Orbital Swap in Li Initiated by Attosecond Pulses. *Ultrafast Sci.* 2023;3:Article 0028. https://doi.org/10.34133/ultrafastscience.0028

Submitted 29 November 2022
Accepted 4 April 2023
Published 5 May 2023

A universal mechanism of ultrafast 2-electron orbital swap is discovered through 2-photon sequential double ionization of Li. After a *1s* electron in Li is ionized by absorbing an extreme ultraviolet photon, the other 2 bound electrons located on 2 different shells have either parallel or antiparallel spin orientations. In the latter case, these 2 electrons are in the superposition of the singlet and triplet states with different energies, forming a quantum beat and giving rise to the 2-electron orbital swap with a period of several hundred attoseconds. The orbital swap mechanism can be used to manipulate the spin polarization of photoelectron pairs by conceiving the attosecond-pump attosecond-probe strategy and thus serves as a knob to control spin-resolved multielectron ultrafast dynamics.

Introduction

Chemical reactions fundamentally rely on dynamics of charged particles in the time scale of femtoseconds or even attoseconds [1]. The advent of attosecond pulses [2] makes it possible to capture ultrafast electron dynamics with unprecedented time resolutions. By tracing electron movies, one is able to discover mechanisms governing ultrafast dynamics. Implementation of these mechanisms to steer ultrafast reactions under strong lasers has been a long aim in attosecond physics [3]. An important way of steering ultrafast reactions would be to launch an electron to multiple coherent states, forming quantum beats that initiate ultrafast charge density oscillations, which may be used to probe electron–electron correlations [4] and control electron localization in molecular dissociation [5,6].

Although a series of ultrafast processes have been explored in multielectron systems, we are still far from a full understanding of ultrafast dynamics in atoms with more than 2 electrons in strong laser fields. The main obstacle is the lack of fully correlated 3-dimensional quantum calculations, which are beyond the capabilities of current computers. A circuitous route is to use the single-active-electron approximation, which is very successful especially when only a valence electron contributes to the main dynamics [7,8]. However, if a multielectron atom is exposed to high-frequency light sources such as x-ray free-electron lasers [9,10] and attosecond pulses [11], an inner-shell electron may be preferentially kicked off, and the shell structure sustained by the Pauli exclusion principle becomes unstable. Therefore, electron correlations become important in multielectron ultrafast processes [12–16]. As the simplest open-shell atom, Li is used as a benchmark to study multielectron effects. Numerical models based on the close-coupling method [17–21] can provide reliable photoionization cross-sections of Li [22–24]. The directly numerical simulations of 1-dimensional time-dependent Schrödinger equation (TDSE) have been used to study spin-resolved strong field ionization [25–27]. Previous works [28–31] showed that the electron spin configuration plays a major role for photoionization dynamics in multielectron systems. However, the main mechanism behind the spin-related conclusions in these works is limited to the photoionization cross-sections in which the scattering dynamics between electrons will be influenced by the spin configurations (the Pauli exclusion principle). One may expect more universal and fundamental mechanisms that can be used to perform ultrafast spin-resolved control for multielectron dynamics.

In this work, we study the spin-selective ionization of Li in attosecond extreme ultraviolet (EUV) pulses and discover a fundamental ultrafast mechanism of 2-electron orbital swap of bound electrons in Li^+. We numerically simulate the TDSE including 3 active electrons initially being prepared in the ground state ($S = 1/2$, $M_S = 1/2$). For atoms in EUV fields, an inner-shell electron always preferentially absorbs an EUV photon if the photon energy is big enough. Once an inner-shell electron absorbs an EUV photon, according to its spin orientation, the residual electrons in Li^+ could be either in the parallel or antiparallel spin state, as depicted in Fig. 1. In the former case, the 2 identical electrons stay in the triplet state ($S = 1$, $M_S = 1$). However, in the latter case of the antiparallel spin state, the 2-electron state cannot be fully described by a single configuration and will actually evolve as a superposition of the singlet ($S = 0$, $M_S = 0$) and the triplet ($S = 1$, $M_S = 0$) states as time flows. Such a quantum beat leads to the periodical

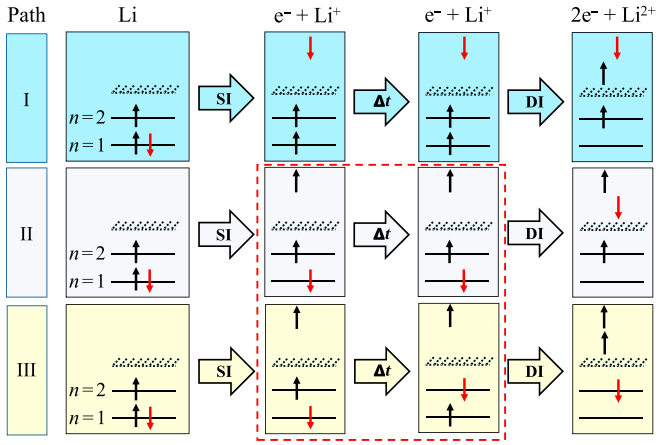

Fig. 1. Schematic diagram of 3 paths for sequential 2-photon DI of 2 inner-shell electrons. In path I, a spin-down inner-shell electron escapes, leaving the 2 bound electrons with the same spin orientation. In path II and path III, Li^+ undergoes orbital swap (surrounded by the red dashed line).

orbital swap of the 2 electrons in Li^+. Note that the orbital here is more like to mean the electron location. Orbital swap actually means the 2 electrons periodically hop between $n = 1$ and $n = 2$ states. In the later time, another inner-shell electron may absorb the second photon and gets freed. There are 2 directly outputs in sequential 2-photon double ionization (DI) of 2 inner-shell electrons according to the orbital swap. First, the time delay of absorbing 2 photons depends on the spin orientations of the first photoelectron. Second, the spin orientations of the second photoelectron can be selected, and thus, it is possible to produce spin-polarized electron pairs with an attosecond pump–probe strategy. In contrast to previous studies about the spin selectivity of the photoelectron [32–36], our demonstration of spin-polarized electron pairs does not rely on the spin-orbit interaction [37] and paves a new way to perform the spin control of photoelectrons with the orbital swap mechanism. In essence, the mechanism discovered in Li is general and exists in other open-shell atoms as well. Such a mechanism makes it possible to control spin-resolved ultrafast processes induced by strong laser fields.

Methods

In Li, the 2 inner-shell electrons couple to the singlet spin state [29], which then couples with the third spin-up electron, forming the state ($S = 1/2$, $M_S = 1/2$) where we have assumed that the outer-shell electron is spin-up before introducing lasers. The 3-electron wave function satisfies the exchange asymmetry and is written as

$$\Psi(q_1,q_2,q_3) = \mathcal{A}\left\{\frac{1}{\sqrt{2}}[\alpha(1)\beta(2)\alpha(3) - \beta(1)\alpha(2)\alpha(3)]\psi(x_1,x_2,x_3)\right\}. \quad (1)$$

Here, q_i is the spin-spatial coordinate, x_i is the spatial coordinate, ψ is the spatial wave function, $\mathcal{A}$ is the antisymmetrization operator, and $\alpha(i)$ and $\beta(i)$ represent spin-up and spin-down states, respectively. After some algebra, the wave function can be reformulated as

$$\Psi(q_1,q_2,q_3) = \Theta\{\alpha(1)\alpha(2)\beta(3)\Phi_{\alpha\alpha\beta}(x_1,x_2,x_3)\}, \quad (2)$$

where Θ performs the cyclic sum $\Theta f(1,2,3) = [f(1,2,3) + f(2,3,1) + f(3,1,2)]/\sqrt{3}$ for arbitrary f. $\Phi_{\alpha\alpha\beta}(x_1,x_2,x_3)$ is the spatial wave function associated with the spin base $\alpha(1)\alpha(2)\beta(3)$, and it is antisymmetric under the exchange of x_1 and x_2. $\Phi_{\alpha\alpha\beta}(x_1,x_2,x_3)$ can be explicitly written as

$$\Phi_{\alpha\alpha\beta}(x_1,x_2,x_3) = \frac{1}{2}[\psi(x_2,x_3,x_1) + \psi(x_3,x_2,x_1) - \psi(x_1,x_3,x_2) - \psi(x_3,x_1,x_2)]. \quad (3)$$

The wave function $\Phi_{\alpha\alpha\beta}$ shows that $e_2^{\uparrow}, e_3^{\downarrow}$ (or $e_1^{\uparrow}, e_3^{\downarrow}$) are in the inner shell and the first (or last) 2 terms of the spatial wave function are symmetric under the exchange of x_2 (or x_1) and x_3, and $e_1^{\uparrow}$ (or $e_2^{\uparrow}$) is in the outer shell.

The ab initio simulation of the TDSE including 3 active electrons in full dimensions demands extraordinarily heavy calculation resources, which is out of the capability of the most advanced computers in the world. To make it feasible, in this study, we use a linearly polarized EUV pulse to interact with Li, and confine the electron movement along the laser polarization direction. The simulation using such a reduced-dimensionality model is still heavy. In 1 dimension, the $n = 1$ and $n = 2$ orbitals can be represented as *1s* and *2p*. Therefore, we express the main configuration of the ground state based on Eq. 3 as

$$\sqrt{2}\Phi_{\alpha\alpha\beta}(x_1,x_2,x_3) = \langle x_2,x_3|1s^2\,{}^1S\rangle\langle x_1|2p\rangle - \langle x_1,x_3|1s^2\,{}^1S\rangle\langle x_2|2p\rangle. \quad (4)$$

Though the 1-dimensional model cannot describe the ionization process accurately and the electron–electron correlation is overestimated, the exchange symmetry characters of the system are preserved. Therefore, the reduced 1-dimensional model can grasp the central physics and qualitatively describe the dynamics we discussed in this paper.

In Eq. 2, different spin bases are orthogonal by definition, and no transition between different spin bases occurs within the dipole approximation. Without loss of generality, we simulate the TDSE under the spin base $\alpha(1)\alpha(2)\beta(3)$ (atomic units are used throughout unless stated otherwise)

$$i\frac{\partial}{\partial t}\Phi_{\alpha\alpha\beta}(x_1,x_2,x_3;t) = [H_0 + W(t)]\Phi_{\alpha\alpha\beta}(x_1,x_2,x_3;t), \quad (5)$$

where the field-free Hamiltonian is

$$H_0 = \sum_{i=1}^{3}\left(-\frac{1}{2}\frac{\partial^2}{\partial x_i^2} - \frac{3}{\sqrt{x_i^2+s^2}}\right) + \sum_{i=1}^{3}\sum_{j=1}^{i-1}\frac{1}{\sqrt{(x_i-x_j)^2+s^2}} \quad (6)$$

with s the soft-core parameter [38] to adjust the ground-state energy in the model. Within the dipole approximation, the laser–Li coupling is expressed as

$$W(t) = \sum_{i=1}^{3}\left[-iA(t)\frac{\partial}{\partial x_i}\right] \quad (7)$$

with $A(t)$ the laser vector potential. The ground state is obtained by imaginary-time propagation of the field-free Schrödinger equation while constraining the trial wave function to have the same exchange property as $\Phi_{\alpha\alpha\beta}$ [39], and the real-time propagation is performed by the Crank–Nicolson method [40]. Our simulation box covers the area of [−439.9,439.9] a.u. in each dimension. This size is big enough to hold all the 2-photon double-ionization events during the whole simulation. The spatial steps are $\Delta x_1 = \Delta x_2 = \Delta x_3 = 0.2$ a.u., and the time step is $\Delta t = 0.05$ a.u. To relieve such heavy 3-dimensional simulations, in real calculations, 1 dimension can be confined in a relatively smaller range when we discuss the double-ionization events propagating along another 2 dimensions. The code is parallelized using OpenMP. Simulation convergence has been tested by using smaller time-spatial grids, and same results are obtained. The ground-state energy −7.477 a.u. is ensured by setting $s = 0.504$. We may point out that the multiconfiguration time-dependent Hartree–Fock method [41] is possible to deal with such a system by treating each electron in 3 dimensions. However, enough configurations must be set to well describe the excited Li^+. In our calculations, the laser vector potential is written as

$$A(t) = A_0 \sin^2\left(\pi t/\tau_{\mathrm{EUV}}\right)\sin(\omega t),\ \ t \in \left[0, \tau_{\mathrm{EUV}}\right]. \quad (8)$$

The central frequency is fixed at $\omega = 5$ a.u., and the laser has an intensity 4.0×10^{16} W/cm^2. Note that the laser intensity is not crucial for the mechanism we discover in this study, and we use the high intensity only for obtaining a better signal-to-noise ratio. In potential experiments in the near future, the EUV intensity can be chosen according to detect enough 2-photon double-ionization signals.

Due to the electron–electron correlation, the ground state of Li $\Phi_{\alpha\alpha\beta}(x_1, x_2, x_3)$ is not the direct product of 3 single-particle states $\psi_{n_1}(x_1)\psi_{n_2}(x_2)\psi_{n_3}(x_3)$ but can be written as

$$\Phi_{\alpha\alpha\beta}\left(x_1, x_2, x_3\right) = \sum_{n_1, n_2, n_3} C_{n_1, n_2, n_3}\psi_{n_1}\left(x_1\right)\psi_{n_2}\left(x_2\right)\psi_{n_3}\left(x_3\right) \quad (9)$$

where $\psi_{nj}(x_j)$ is the eigenstate of 1-dimensional Li^{2+}. C_{n_1, n_2, n_3} is the amplitude, and it shows the main configuration of the ground state in the single-particle bases. $\psi_{n_j}(x_j)$ can be obtained by solving the stationary Schrödinger equation for Li^{2+}

$$\left[-\frac{1}{2}\frac{\partial^2}{\partial x_j^2} - \frac{3}{\sqrt{x_j^2 + s^2}}\right]\psi_{n_j}\left(x_j\right) = E_{n_j}\psi_{n_j}\left(x_j\right). \quad (10)$$

The probability for $\Phi_{\alpha\alpha\beta}(x_1, x_2, x_3)$ on $\psi_{n_1}(x_1)\psi_{n_2}(x_2)\psi_{n_3}(x_3)$ is $|C_{n_1, n_2, n_3}|^2$. Similarly, by removing 1 electron in Eq. 5 and following the same procedure as that done for Eq. 10, one may calculate the Eigen energies for Li^+. In Table 1, we show the energy levels of our model for Li, Li^+, and Li^{2+} in different states. In the last 4 rows in the table, "×" means no constraint on this spatial wave function. The data in Table 2 demonstrate that $e_3^{\downarrow}$ must be on the inner shell (occupy the *1s* orbit), and the other 2 spin-up electrons are located on different shells (mainly on *1s* and *2p* states). Thus, the expression of Eq. 4 makes sense.

Table 1. Energy levels of 1-dimensional targets.

Target	Configuration	S	Energy (a.u.)
Li	$1s^2 2p$	$\frac{1}{2}$	−7.477
Li^+	$1s^2$	0	−7.098
Li^+	*1s2p*	1	−5.472
Li^+	*1s2p*	0	−5.207
Li^{2+}	*1s*	$\frac{1}{2}$	−4.267
Li^{2+}	*2p*	$\frac{1}{2}$	−2.027

Table 2. Projection of $\Phi_{\alpha\alpha\beta}(x_1, x_2, x_3)$ onto single-particle states.

$\|\psi_{n_1}\rangle$	$\|\psi_{n_2}\rangle$	$\|\psi_{n_3}\rangle$	$\|C_{n_1, n_2, n_3}\|^2$
$\|1s\rangle$	$\|1s\rangle$	$\|1s\rangle$	$<10^{-10}$
$\|1s\rangle$	$\|2p\rangle$	$\|1s\rangle$	0.367
$\|2p\rangle$	$\|1s\rangle$	$\|1s\rangle$	0.367
$\|2p\rangle$	$\|2p\rangle$	$\|1s\rangle$	$<10^{-10}$
$\|1s\rangle$	$\|1s\rangle$	$\|2p\rangle$	$<10^{-10}$
$\|1s\rangle$	$\|2p\rangle$	$\|2p\rangle$	$<10^{-10}$
$\|2p\rangle$	$\|1s\rangle$	$\|2p\rangle$	$<10^{-10}$
$\|2p\rangle$	$\|2p\rangle$	$\|2p\rangle$	$<10^{-10}$
×	×	$\|1s\rangle$	0.992
×	×	$\|2p\rangle$	0.004
$\|1s\rangle$	×	×	0.493
$\|2p\rangle$	×	×	0.376

Results and Discussion

Single ionization of Li

The study of single ionization can lay a foundation for our research on DI. By simulating the TDSE including 3 active electrons, we may trace the wave function evolution with time. At the end of the calculation, we collect the wave function in the area ($|x_1| > 30$ a. u., $|x_2| < 30$ a. u., $|x_3| < 30$ a. u.), or ($|x_1| < 30$ a. u., $|x_2| > 30$ a. u., $|x_3| < 30$ a. u.) or ($|x_1| < 30$ a. u., $|x_2| < 30$ a. u., $|x_3| > 30$ a. u.), and transform them to momentum representation to get the momentum distribution. Figure 2A and B shows the photoelectron momentum distributions in the positive half spaces using the laser pulse durations of 100 and 38 a.u., respectively. In both panels, the solid and dotted curves are for $e_1^{\uparrow}$ and $e_3^{\downarrow}$, respectively. The dotted curve in Fig. 2A mainly presents 2 peaks. This is understandable with the help of Table 2. The emission of $e_3^{\downarrow}$, which must be in the *1s* shell, leaves Li^+ in the $|1s2p^3P\rangle$ state or even higher excited states. If the ion is in the $|1s2p^3P\rangle$ state, the momentum of the emitting electron is $\sqrt{2\left(\omega - I_P^A\right)}$ a.u., where I_P^A is the potential to ionize Li to Li^+ in the $|1s2p^3P\rangle$ state. As shown in Table 1, $I_P^A = 2.005$ a.u., and thus the momentum is equal to 2.45 a.u., which is coincident

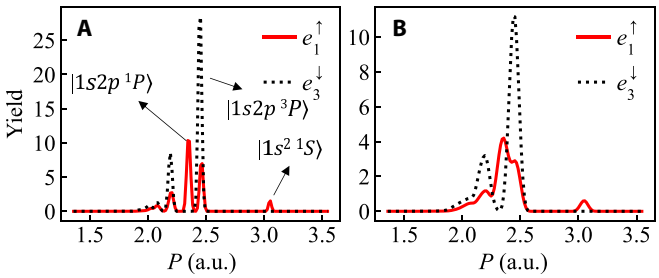

Fig. 2. Photoelectron momentum spectra (only the positive parts) for the single ionization of Li when the laser pulse duration is (A) 100 a.u. and (B) 38 a.u. Each panel is normalized by the single-ionization rate of $e_1^{\uparrow}$.

with the highest peak of the dotted line in Fig. 2A. Alternatively, after $e_3^{\downarrow}$ absorbs a photon, it may excite another electron via electron–electron correlation, i.e., the single photon energy is shared between $e_3^{\downarrow}$ and the outer-shell electron. Such a process contributes the momentum peak at 2.2 a.u.

The emission of $e_1^{\uparrow}$ brings more complex structures. $e_1^{\uparrow}$ can be in either the *1s* or *2p* shell, and thus has different ionization potentials. For $e_1^{\uparrow}$ in the *2p* shell, its ionization potential is $I_p^1 = 0.379$ a.u. in our 1-dimensional model, and thus, the photoionization gives the momentum $\sqrt{2\left(\omega - I_p^1\right)} = 3.04$ a.u. Note that this peak is missing in the dotted curve since $e_3^{\downarrow}$ cannot be in the outer shell. On the other hand, if $e_1^{\uparrow}$ is in the inner shell, the emission of $e_1^{\uparrow}$ leaves Li^+ in the superposition of $|1s2p^3P\rangle$ and $|1s2p^1P\rangle$. Since $|1s2p^3P\rangle$ and $|1s2p^1P\rangle$ are spatially exchange symmetry and antisymmetry, the electron–electron correlation is different and the 2 states have different energies. Indeed, the 2 peaks at 2.34 and 2.45 a.u. correspond to Li^+ in the $|1s2p^1P\rangle$ and $|1s2p^3P\rangle$ states, respectively. As one can clearly see, the peak at 3.04 a.u. is much lower than others, which is due to the fact that the inner-shell electron is preferential to absorb highly energetic photons [28,29]. When a pulse with a short duration is used, the laser spectrum width is wider and cannot resolve the energy gap between $|1s2p^3P\rangle$ and $|1s2p^1P\rangle$ states. In that case, 2 peaks merge at around 2.40 a.u., as shown in Fig. 2B.

Two-electron joint momentum distributions

In the study of DI, we look into the joint momentum distribution (take $p_1 - p_2$ as an example). We collect the wave function in the area $|x_1| > 30$ a.u., $|x_2| > 30$ a.u., and $|x_3| < 30$ a.u. at the end of the simulation $t = t_f$, and partially Fourier transform it with respect to x_1 and x_2 to obtain $\widetilde{\Phi}_{1,2}(p_1, p_2, x_3, t_f)$. The projection $\langle p_1, p_2, \psi_n | \widetilde{\Phi}_{1,2}(t_f) \rangle$ gives the amplitude that 2 electrons have the momentum (p_1, p_2), and meanwhile, Li^{2+} is in the 1-electron orbital $\psi_n(x_3)$. In this section, we resolve the sequential inner-shell double-ionization paths for the electron pairs with different spin states and extract the channel induced by the orbital swap mechanism.

Figure 3A and B shows the $e_1^{\uparrow}e_2^{\uparrow}$ and $e_1^{\uparrow}e_3^{\downarrow}$ joint momentum distributions for 2-photon DI with Li^{2+} in its first excited state, respectively. In both panels, the events that we collect are distributed on the circle $p_1^2/2 + p_{2,3}^2/2 = 2\omega - I_p$, where I_p is the energy threshold to free 2 inner-shell electrons. To show their differences more clearly, we integrate the events in Fig. 3A and

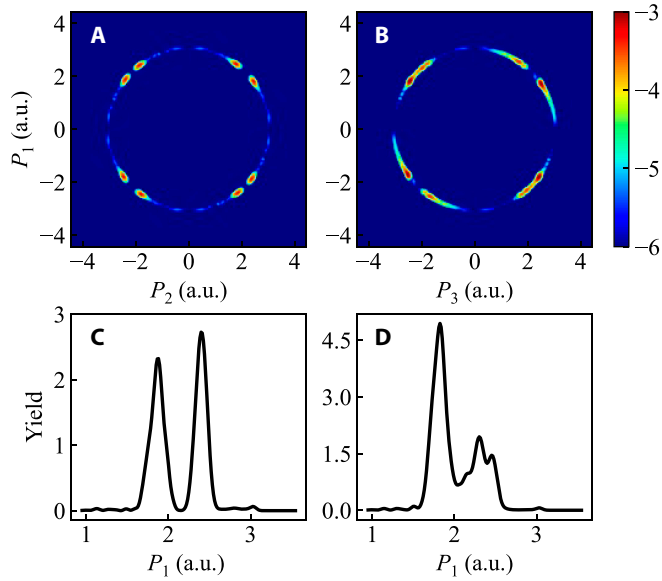

Fig. 3. (A and B) Correlated momentum spectra (in logarithmic scale) for 2-photon DI (the ion stays in its first excited state) of $e_1^{\uparrow}e_2^{\uparrow}$ and $e_1^{\uparrow}e_3^{\downarrow}$, respectively. (C and D) $e_1^{\uparrow}$ momentum distributions obtained by integrating the events in the second quadrant in (A) and (B) along the horizontal axis, respectively. The EUV pulse duration is 38 a.u.

B along the horizontal axis to plot the momentum distribution of the electron $e_1^{\uparrow}$, as shown in Fig. 3C and D. Both curves present 2 clear peaks at around 1.85 and 2.4 a.u. The peaks at 2.4 a.u. in all panels are trivial, i.e., $e_1^{\uparrow}$ absorbs 1 photon and is ionized from the inner shell (see in Fig. 2). To produce the peak at 1.85 a.u. in Fig. 3D, $e_3^{\downarrow}$ is firstly ionized by absorbing a photon, and then the inner-shell $e_1^{\uparrow}$ is sequentially released by absorbing the second photon. This scenario can be derived from the energy diagrams of Li and Li^+ shown in Table 1. The above analysis establishes that Li absorbs 2 photons sequentially. For double ionization (DI) of $e_1^{\uparrow}$ and $e_3^{\downarrow}$, the peak around 1.85 a.u. is much higher than that around 2.4 a.u. in Fig. 3D, which shows that $e_1^{\uparrow}$ has a larger probability to absorb the second photon, i.e., path I in Fig. 1 dominates. However, for DI of $e_1^{\uparrow}e_2^{\uparrow}$, the 2 electrons have the same spin and are located on different shells initially, which seems to be contradictory to the previously mentioned mechanism requiring the photoionization of 2 inner-shell electrons. A possible way to meet the energy diagram is that the inner-shell $e_3^{\downarrow}$ absorbs the second photon and knocks out the outer-shell spin-up electron on its way out. However, such a pathway, similar to the well-known "shake off" process, has small cross-section especially when the driving laser pulse is not too short. This scenario can be excluded by numerical simulations, which are to be discussed in Fig. 5. Hence, to simultaneously meet the spin and energy requirement, the outer-shell electron must fill the hole in the inner shell in some manner once the spin-up inner-shell electron has been ionized by absorbing the first photon. Hence, the 2 electrons on 2 different shells in Li^+ must swap their orbitals, which is the so-called orbital swap mechanism in order to preserve the energy conservation after the single ionization. When the outer-shell spin-up electron hops to the inner shell, it can absorb another photon, contributing to the peak around 1.85 a.u. in Fig. 3C. This scenario is described by path III in Fig. 1, ending with the 2 photoelectrons in the spin-triplet state.

Streaking photoelectron spectra

In the above section, we claim that Li absorbs 2 EUV photons sequentially. This statement is confirmed by photoelectron energy spectra in Fig. 3. However, the best way to support the sequential absorption of 2 photons is by investigating the streaking spectrogram of photoelectrons [42,43]. In this subsection, we use the 1-cycle (to ensure that our simulation box can hold all the 2-photon double-ionization wave packets) 1,200-nm laser pulse with the intensity 5.0×10^{11} W/cm^2 to streak the double-ionization events. Approximately, the final photoelectron momentum under the streaking field can be written as

$$\vec{p}\left(t_f\right) = \vec{p}_0 - \vec{A}_s\left(\tau_s + \Delta t_s\right), \tag{11}$$

where the streaking laser vector potential is

$$\vec{A}_s\left(\tau_s\right) = \vec{A}_0 \sin^2\left[\pi\left(\tau_s + 0.5T_s\right)/T_s\right]\cos\left(\omega_s \tau_s\right). \tag{12}$$

Here, τ_s is the time delay between the center of the EUV pulse and the center of the streaking field, and T_s is the period of the streaking field. Δt_s is the streaking time delay, and $\vec{p}_0$ is the photoelectron momentum when the streaking field is absent. By fitting the simulation results with Eq. 11, we can get the streaking time delay. A negative (positive) time delay means that the photon is absorbed before (after) the center of the EUV pulse. In Fig. 4A and C, we show the streaking spectrograms (DI of $e_1^{\uparrow}e_2^{\uparrow}$) for 2 electrons emitting along the same and opposite directions, respectively. Our simulation for both cases shows that the traces at the high-momentum peak (around 2.4 a.u.) and the low-momentum peak (around 1.85 a.u.) have time delays of about −5.0 and 4.5 a.u., respectively, as marked by the vertical dashed lines in each panel. These results confirm the sequential 2-photon ionization scenarios. The time interval of absorbing the first and second photons relies on the EUV pulse duration [43]. Different from the sequential DI of He in [43], our 2-photon absorption delay will also be influenced by the orbital swap mechanism. For instance, for DI of $e_1^{\uparrow}e_3^{\downarrow}$, the streaking delay of $e_1^{\uparrow}$ for the peak around 1.85 a.u. is about 3.5 a.u., as shown in Fig. 4B and D, which is smaller than the value in DI of $e_1^{\uparrow}e_2^{\uparrow}$. Such a difference can be explained as follows. For DI of $e_1^{\uparrow}e_2^{\uparrow}$, after $e_1^{\uparrow}$ is emitted, Li^+ needs some time to accomplish the orbit swap between $e_2^{\uparrow}$ and $e_3^{\downarrow}$. The second-photon absorption occurs after $e_2^{\uparrow}$ and $e_3^{\downarrow}$ swap. The streaking time difference for DI of $e_1^{\uparrow}e_2^{\uparrow}$ and $e_1^{\uparrow}e_3^{\downarrow}$ has not been studied before, and it carries the information of correlated electrons, which deserves to be studied further.

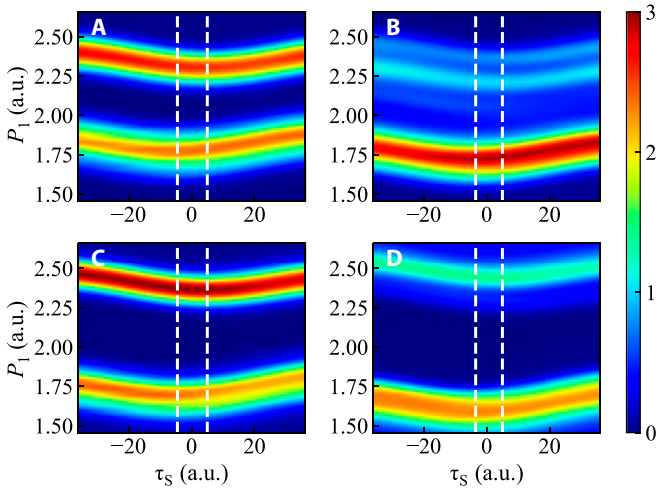

Fig. 4. The streaking spectrogram of $e_1^{\uparrow}$ along the positive direction under different conditions. (A and B) Two electrons emit along the same direction. (C and D) Two electrons emit along opposite directions. The left and right columns are for the double-ionization events of $e_1^{\uparrow}e_2^{\uparrow}$ and $e_1^{\uparrow}e_3^{\downarrow}$, respectively. The 1-cycle 1,200-nm streaking infrared field has the intensity 5.0×10^{11} W/cm^2. The white dashed lines mark the troughs of the streaked patterns.

Inelastic scattering in DI

According to the photoelectron momentum distribution and streaking spectrogram, it is the 2 inner-shell electrons that absorb 2 photons and get freed. It is intuitive to have 2 photoelectrons with opposite spins since the 2 inner-shell electrons automatically satisfy all requirements. However, obtaining 2 photoelectrons with the same spin sounds contradict to the initial condition since these 2 electrons distribute on 2 different shells. Besides the orbital swap, another plausible way to meet the energy diagram is the following. After $e_1^{\uparrow}$ is released, $e_3^{\downarrow}$ in the inner shell may absorb the second photon. During its way out, $e_3^{\downarrow}$ knocks out the out-shell electron $e_2^{\uparrow}$ and itself is captured in the outer shell. In this way, the 2 photoelectrons are both

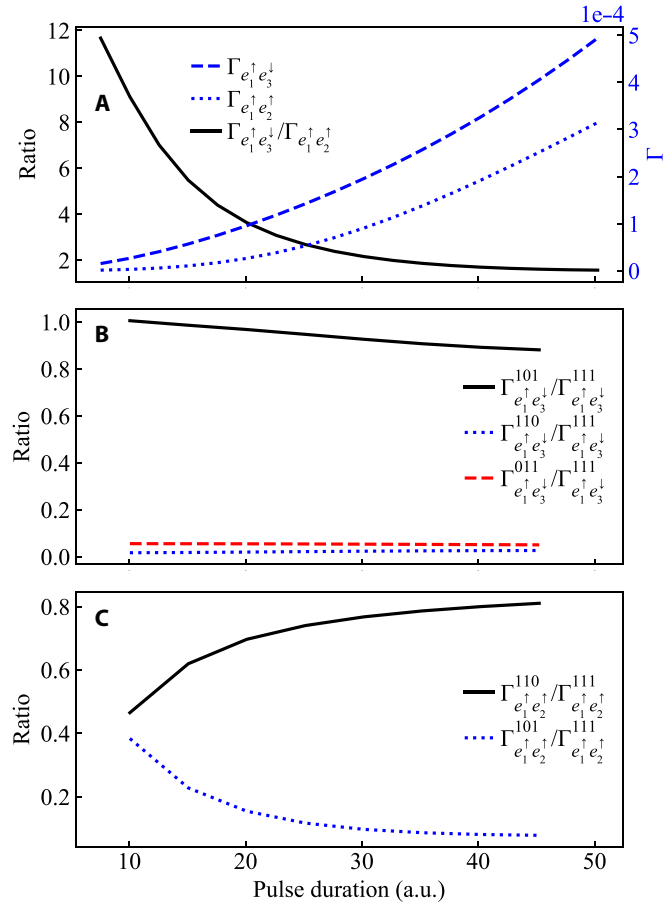

Fig. 5. (A) The 2-photon DI probability with Li^{2+} in its first excited state as a function of the laser pulse duration. The blue dotted and dashed lines are for $e_1^{\uparrow}e_2^{\uparrow}$ and $e_1^{\uparrow}e_3^{\downarrow}$, respectively. The black solid line shows the ratio of the two. (B and C) The double-ionization probabilities obtained by selectively setting one of $f_i = 0$ as a function of the pulse duration.

spin up, and their joint momentum distributions would be similar as shown in Fig. 3. However, in this section, we will show such a pathway only is nonnegligible when the driving laser pulse is extremely short. Usually, this pathway can be excluded due to very tiny probabilities.

To explore how the photon energy deposits into Li, we artificially revise the laser–electron coupling term by adding 3 parameters (f_1, f_2, f_3) into the dipole interaction to turn on ($f_i = 1$) or turn off ($f_i = 0$) the interaction for a certain electron with the laser field

$$W(t) = A(t)\left(f_1 p_1 + f_2 p_2 + f_3 p_3\right). \tag{13}$$

By investigating the f_j-dependent double-ionization rate, one can estimate the importance of electron–electron Coulomb correlation in DI. First, we include the full laser–electron coupling, i.e., $f_1 = f_2 = f_3 = 1$, and show the ratio between the ionization rates of $e_1^{\uparrow}e_2^{\uparrow}$ and $e_1^{\uparrow}e_3^{\downarrow}$ in Fig. 5A. The sensitive dependence of the ratio on the pulse duration indicates that the ionization mechanisms are different for different pulse duration. Then, by turning off part of the laser–electron interaction, we can realize the importance of the laser–electron interaction and, on the contrary, the importance of the complementary electron–electron correlation. Figure 5B and C shows the ionization probability as a function of the laser pulse duration. The 3 parameters marked in the superscript of the ionization probability ($\Gamma^{f_1 f_2 f_3}$) are used to express the results under different laser–Li interactions. From Fig. 5B, for DI of $e_1^{\uparrow}e_3^{\downarrow}$, the main double-ionization channel is the photon absorption of the 2 inner-shell electrons ($e_1^{\uparrow}$ and $e_3^{\downarrow}$), and other channels that need inelastic scattering between electrons have a negligible probability. This supports the main mechanism for DI of $e_1^{\uparrow}e_3^{\downarrow}$ (path I in Fig. 1).

For DI of $e_1^{\uparrow}e_2^{\uparrow}$, as presented in Fig. 5C, we find that the main channel originates from the photon absorption of $e_1^{\uparrow}$ and $e_2^{\uparrow}$ when the pulse duration is not very short, which also excludes the inelastic channel for these parameters. When the pulse duration is very short, the probability of the sequential photon absorption channel for DI of $e_1^{\uparrow}e_2^{\uparrow}$ ($\Gamma^{110}_{e_1^{\uparrow}e_2^{\uparrow}}$) has the same order of magnitude with the inelastic scattering channel ($\Gamma^{101}_{e_1^{\uparrow}e_2^{\uparrow}}$). However, the contribution of the inelastic scattering channel is usually much smaller than the normal sequential 2-photon process (path I), as shown by the black-solid curve in Fig. 5A. With the increasing of the laser pulse duration, the proportion of the inelastic scattering channel is smaller. Based on our analysis above, we can deduce that the channels that need inelastic scattering are not the main channel for 2-photon DI with excitation in this work. For the sequential photon absorption channel for DI of $e_1^{\uparrow}e_2^{\uparrow}$, there should be a certain time delay between the sequential 2-photon absorption to wait for the orbit swap happens, and a very short laser pulse does not favor the mechanism.

Formulating the orbital swap mechanism

Above simulation results all support the orbital swap of 2 electrons in Li^+ after single ionization. In this subsection, we formulate the orbital swap. Physically, the ground state can be rewritten as [29]

$$\begin{aligned}\sqrt{2}\Phi_{\alpha\alpha\beta}(x_1,x_2,x_3) &= \langle x_1,x_3|1s^2\,{}^1S\rangle\langle x_2|2p\rangle \\ &+ \frac{1}{\sqrt{2}}\left[\langle x_1,x_3|1s2p^3P_{M_S=0}\rangle - \langle x_1,x_3|1s2p^1P\rangle\right]\langle x_2|1s\rangle.\end{aligned} \tag{14}$$

This expression can be confirmed by the single-ionization spectra in Fig. 2. If the *1s*-electron $e_2^{\uparrow}$ is removed at t_1, the remaining Li^+ will be in the superimposed state consisting of the triplet state $|A\rangle = |1s2p\,{}^3P_{MS=0}\rangle$ and the singlet state $|B\rangle = |1s2p\,{}^1P\rangle$. One can expand the spatial wave functions of the 2 states with 1-dimensional Li^+ orbitals ϕ_n as

$$\begin{aligned}\sqrt{2}\langle x_1,x_3\,|\,A\rangle &= \phi_{1s}(x_1)\phi_{2p}(x_3) - \phi_{1s}(x_3)\phi_{2p}(x_1), \\ \sqrt{2}\langle x_1,x_3\,|\,B\rangle &= \phi_{1s}(x_1)\phi_{2p}(x_3) + \phi_{1s}(x_3)\phi_{2p}(x_1).\end{aligned} \tag{15}$$

To complete the derivation, we assume the photoelectron is in plane wave orbitals $|\epsilon\rangle$ and rewrite the wave function of the (Li^+,e^-) system produced at t_1 after the emitting of $e_2^{\uparrow}$

$$\begin{aligned}|\Psi_{t_1}(t)\rangle = \int d\varepsilon\,|\,\varepsilon\rangle e^{-i\varepsilon(t-t_1)}\{\,|\,A\rangle C_{t_1}\left(E_A+\epsilon\right)e^{-iE_A(t-t_1)} \\ + |\,B\rangle C_{t_1}\left(E_B+\epsilon\right)e^{-iE_B(t-t_1)}\}.\end{aligned} \tag{16}$$

Here, E_A and E_B are energies of $|A\rangle$ and $|B\rangle$ states (see Table 1), and $|C_{t_1}(E)|^2$ is the energy distribution centered at $E = E_{gs} + \omega$ (E_{gs} is the ground-state energy), which is determined mainly by the photon energy bandwidth. In the extreme case that the single ionization is triggered by a delta pulse at t_1, which is similar to the sudden removal of an inner-shell electron, $C_{t_1}(E)$ would have infinite width and $C_{t_1}(E_A + \epsilon) \approx C_{t_1}(E_B + \epsilon)$. By projecting Eq. 16 onto $|2p, \varepsilon, 1s\rangle$ and integrating over ε, one can obtain the probability of the spin-down electron being in the inner shell

$$P_{\beta}^{1s}(t) \propto \cos^2\left[\Delta E\,(t-t_1)/2\right]. \tag{17}$$

Equation 17 indicates that the period of orbital swap is $T = 2\pi/\Delta E$. In our 1-dimensional model, this period is about 24 a.u. We further emphasize that we neglect the laser-spin coupling in this study since it is much smaller. It is the mechanism of orbital swap that causes this oscillation and provides a unique opportunity to control the ionization pathways. Note that ΔE in our 1-dimensional model is larger than that in the real 3-dimensional atom; however, this model already explores the mechanism without a doubt.

Time-resolved orbital swap dynamics

If the driving laser pulse duration is longer than the orbital swap period, the 2-electron swap may play an important role in 2-photon ID. To see that, we perform the simulation using a longer laser pulse ($\tau = 100$ a.u.) and diagnose the DI for $e_1^{\uparrow}e_2^{\uparrow}$. Figure 6A presents the wave function distribution at the end of the simulation for DI of $e_1^{\uparrow}$ and $e_2^{\uparrow}$ associating with the Li^{2+} in its first excited state. One can clearly see spatially separated wave packets guided by the white dotted curves. The intercepts of the white dotted line to $x_2 = 0$ are the propagation distances of the first ionized electron just before Li^+ absorbs the second photon. Since the momentum of the first ionized electron is given, the time interval between absorbing the first and second photons ($t_2 - t_1$) can be numerically extracted easily, as shown in Fig. 6C. One may expect more peaks if the driving laser pulse duration is even longer. The maxima appear around $t_2 - t_1 = \left(j - \frac{1}{2}\right)T$ (j is a positive integer) when $e_3^{\downarrow}$ hops to the $n = 2$ shell. This numerical result has a good quantitative agreement with the theoretical prediction. For DI of $e_1^{\uparrow}e_2^{\uparrow}$, the

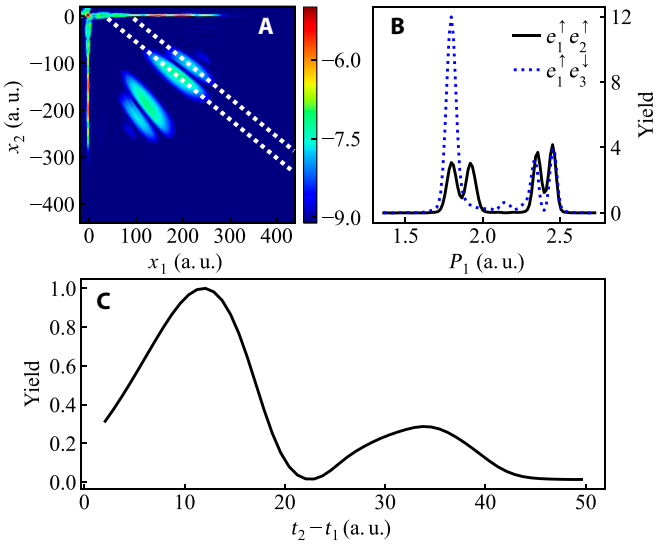

Fig. 6. (A) The wave function distribution (in logarithmic scale) for DI (the ion stays in its first excited state) of $e_1^\uparrow e_2^\uparrow$ at $t = t_f$. (B) $e_1^\uparrow$ momentum spectra (normalized by the DI probability of $e_1^\uparrow e_2^\uparrow$) for DI of $e_1^\uparrow e_2^\uparrow$ (black solid) and $e_1^\uparrow e_3^\downarrow$ (blue dotted). (C) The distribution of the time difference between absorbing the first and second photons. The pulse duration is 100 a.u.

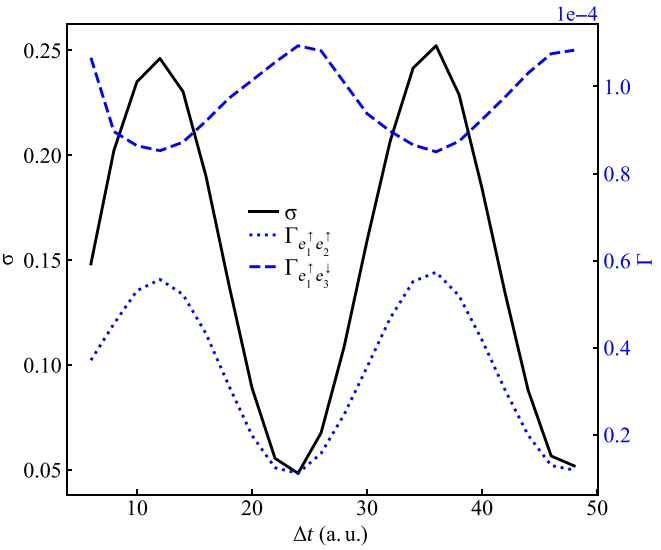

Fig. 7. The spin polarization σ and the 2-photon DI probabilities of $e_1^\uparrow e_2^\uparrow$ and $e_1^\uparrow e_3^\downarrow$ as a function of the time delay between 2 attosecond pulses. Each pulse duration is 10 a.u.

photon energy bandwidth is narrow enough to resolve ΔE and thus 2 subpeaks for $e_1^\uparrow$ around 2.4 a.u. appear, as shown in Fig. 6B. These 2 subpeaks correspond to leaving Li^+ in the $|A\rangle$ and $|B\rangle$ states after absorbing the first photon. The 2 subpeaks at around 1.8 a.u. correspond to the ionization of the *1s* electron of Li^+ from the $|A\rangle$ and $|B\rangle$ superposition by absorbing the second photon. For DI of $e_1^\uparrow e_3^\downarrow$, the emission of $e_3^\downarrow$ only produces Li^+ in the spin-triplet state, and thus, no subpeaks at 1.8 a.u. appear.

Generating spin-polarized electron pairs

The orbital swap mechanism can help us control the ultrafast photoionization dynamics. Here, we show that the principle of the intrinsic orbital swap in Li^+ can be applied to produce spin-selective photoelectron pairs. Previous works showed that one can generate spin-polarized electron pairs through the electron impact [44,45]. Here, we use 2 sequential attosecond pulses to generate the spin-polarized photoelectron pair in the DI of Li. The first attosecond pulse kicks off a spin-up inner-shell electron, leading to the 2-electron orbital swap in Li^+, as described by Eq. 17. If the second attosecond pulse arrives when the spin-up electron hops to the inner shell, another spin-up photoelectron is emitted. Thus, we obtain the 2 correlated electrons in the triplet state. On the contrary, if the second attosecond pulse arrives when the spin-down electron swaps to the inner shell, one obtains 2 photoelectrons with opposite spins. In simulations, the laser field is composed of 2 identical attosecond pulses, and each one is expressed by Eq. 8. Each pulse duration is $\tau_{EUV} = 10$ a.u., and the time delay between 2 attosecond pulses is variable. In Fig. 7, we present the double-ionization probabilities $\Gamma_{e_1^\uparrow e_2^\uparrow}$ and $\Gamma_{e_1^\uparrow e_3^\downarrow}$ with Li^{2+} in its first excited state. We define the spin polarization as

$$\sigma = \frac{\Gamma_{e_1^\uparrow e_2^\uparrow}}{\Gamma_{e_1^\uparrow e_2^\uparrow} + \Gamma_{e_1^\uparrow e_3^\downarrow} + \Gamma_{e_2^\uparrow e_3^\downarrow}}. \quad (18)$$

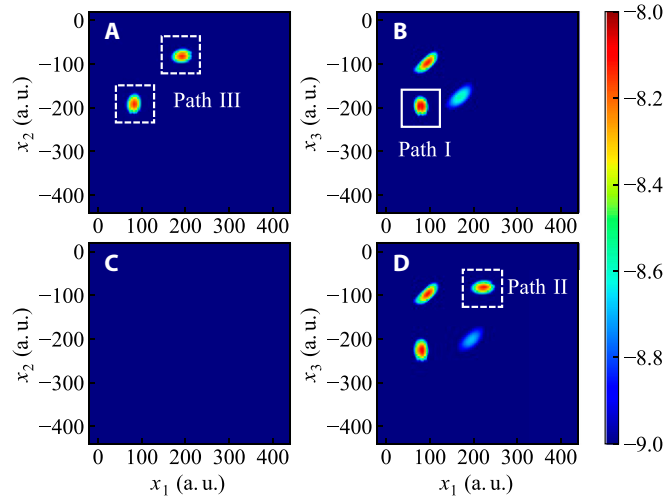

Fig. 8. The wave function distributions (in logarithmic scale) at the end of the calculations when the time delays between 2 attosecond pulses are (A and B) $\Delta t = 36$ a.u. and (C andD) $\Delta t = 48$ a.u. The left and right columns are for DI of $e_1^\uparrow e_2^\uparrow$ and $e_1^\uparrow e_3^\downarrow$, respectively. The duration of each pulses is 10 a.u., the central frequency is $\omega = 5$ a.u., and the intensity is 4.0×10^{16} W/cm^2.

Note that $\Gamma_{e_1^\uparrow e_3^\downarrow} = \Gamma_{e_2^\uparrow e_3^\downarrow}$ due to the identity of $e_1^\uparrow$ and $e_2^\uparrow$. The spin polarization is plotted by the black-solid curve in Fig. 7. Both $\Gamma_{e_1^\uparrow e_2^\uparrow}$ and $\Gamma_{e_1^\uparrow e_3^\downarrow}$, as well as the spin polarization vary with the time delay, and the variational period is same as the 2-electron swap period in Li^+. However, the total double-ionization probability $\Gamma_{e_1^\uparrow e_2^\uparrow} + 2\Gamma_{e_1^\uparrow e_3^\downarrow}$ keeps unchanged.

To better understand the double-ionization dynamics, in Fig. 8, we show the snapshots of the final DI with excitation wave function distributions when the time delays between the 2 attosecond pulses are 36 a.u. (upper row) and 48 a.u. (lower row). The left and right columns present DI of $e_1^\uparrow e_2^\uparrow$ and $e_1^\uparrow e_3^\downarrow$, respectively. In Fig. 8A, the wave packets come from path III. In Fig. 8B, the wave packets along the diagonal come from

the direct emitting of the 2 inner-shell electrons by absorbing 2 photons from the single pulse. The wave packet in the left lower corner comes from path I. The main signals at this time delay (36 a.u., half integrals of the period) will not be affected by the time delay, and we can regard them as the background signals for DI of $e_1^{\uparrow}e_3^{\downarrow}$, which limit the maximum value of the spin polarization parameter σ. When the delay is 48 a.u., only path I and path II exist, thus, the double-ionization probability for $e_1^{\uparrow}e_2^{\uparrow}$ is too small to be visible, as shown in Fig. 8C. Path I and path II contribute to the signals in Fig. 8D. By changing the time delay, the ratio of the ionization probabilities between path II ($e_1^{\uparrow}e_3^{\downarrow}$) path III ($e_1^{\uparrow}e_2^{\uparrow}$) can be controlled.

Conclusion

In summary, we reveal an unexplored orbital swap mechanism by investigating the DI of Li in attosecond EUV pulses. Depending on the photoelectron spin orientation in single ionization of Li, Li^+ may be in the superposition with spatial exchange symmetry and antisymmetry. Such a quantum beat forces the 2 bound electrons in Li^+ to swap their orbitals periodically. By characterizing and precisely timing the ultrafast orbital swap dynamics, one may directly control the spin polarization of the photoelectron pair by the attosecond-pump attosecond-probe strategy [2,46].

The difficulty of directly observing the orbital swap process lies on measuring both photoelectron spin orientations simultaneously on top of the COLTRIMS measurement, which is a technology still under developing. However, this difficulty can be partly relieved by only measuring 1 photoelectron spin. In the 2-photon sequential DI, the secondly released electron has lower energy compared to the firstly released electron. As discussed above, not only the spin polarization of the electron pair but also the spin polarization of the secondly released electron oscillates with the time delay. Therefore, we can use the time-of-flight spectrometer to distinguish the secondly released electrons with lower energies and the spin polarization can be measured by the time-of-flight–Mott spectrometer [35]. With this strategy, we can avoid measuring the spin orientations of the 2 photoelectrons simultaneously.

The orbital swap mechanism can even be confirmed without measuring any photoelectron spin. Since the orbital swap will inevitably determine other process, for example, the high-harmonic generation, we can retrieve the orbtial swap from the high-harmonic spectra. For example, exposing Li in combined EUV and midinfrared laser pulses, an inner-shell spin-up electron is knocked out by the EUV pulse and then driven back to Li^+. The rescattering process may be severely modulated by the orbital swap mechanism. If the photoelectron excursion time is half integers of the swap period, the dipole is annihilated and no harmonics emit. By diagnosing the fine structures in the harmonic spectra, one is possible to retrieve the ultrafast orbital swap. The orbital swap mechanism discovered in this study advances our understanding of atoms with open-shell structures, and more ultrafast spin-resolved dynamics in multielectron systems can be explored in the future.

Acknowledgments

Simulations were performed on the π supercomputer at Shanghai Jiao Tong University. **Funding:** This work was supported by the National Natural Science Foundation of China (NSFC) (Grant No. 11925405 and No. 12274294) and the National Key R&D Program of China (2018YFA0404802). **Competing interests:** There is no conflict of interest regarding the publication of this article.

Data Availability

The data that support the plots within this article and other findings of this study are available from the corresponding author upon reasonable request.

References

1. Nisoli M, Decleva P, Calegari F, Palacios A, Martin F. Attosecond electron dynamics in molecules. *Chem Rev*. 2017;117(16):10760–10825.
2. Chini M, Zhao K, Chang Z. The generation, characterization and applications of broadband isolated attosecond pulses. *Nat Photonics*. 2014;8:178–186.
3. Krausz F, Ivanov M. Attosecond physics. *Rev Mod Phys*. 2009;81:163–234.
4. Hu SX, Collins LA. Attosecond pump probe: Exploring ultrafast electron motion inside an atom. *Phys Rev Lett*. 2006;96:073004.
5. He F, Ruiz C, Becker A. Control of electron excitation and localization in the dissociation of H_2^+ and its isotopes using two sequential ultrashort laser pulses. *Phys Rev Lett*. 2007;99(8):083002.
6. Sansone G, Kelkensberg F, Pérez-Torres JF, Morales F, Kling MF, Siu W, Ghafur O, Johnsson P, Swoboda M, Benedetti E, et al. Electron localization following attosecond molecular photoionization. *Nature*. 2010;465:763–766.
7. Sheehy B, Martin JDD, DiMauro LF, Agostini P, Schafer KJ, Gaarde MB, Kulander KC. High harmonic generation at long wavelengths. *Phys Rev Lett*. 1999;83:5270.
8. Gaarde MB, Schafer KJ, Kulander KC, Sheehy B, Kim D, DiMauro LF. Strong species dependence of high order photoelectron production in alkali metal atoms. *Phys Rev Lett*. 2000;84:2822–2825.
9. Pellegrini C, Marinelli A, Reiche S. The physics of x-ray free-electron lasers. *Rev Mod Phys*. 2016;88:015006.
10. Seddon EA, Clarke JA, Dunning DJ, Masciovecchio C, Milne CJ, Parmigiani F, Rugg D, Spence JCH, Thompson NR, Ueda K, et al. Short-wavelength free-electron laser sources and science: A review*. *Rep Prog Phys*. 2017;80:115901.
11. Duris JP, Li S, Driver T, Champenois EG, MacArthur JP, Lutman AA, Zhang Z, Rosenberger P, Aldrich JW, Coffee R, et al. Tunable isolated attosecond x-ray pulses with gigawatt peak power from a free-electron laser. *Nat Photonics*. 2019;14:30–36.
12. Li S, Driver T, Rosenberger P, Champenois EG, Duris J, al-Haddad A, Averbukh V, Barnard JCT, Berrah N, Bostedt C, et al. Attosecond coherent electron motion in auger-meitner decay. *Science*. 2022;375:285–290.
13. Pabst S, Santra R. Strong-field many-body physics and the giant enhancement in the high-harmonic spectrum of xenon. *Phys Rev Lett*. 2013;111:233005.
14. Faccialà D, Pabst S, Bruner BD, Ciriolo AG, de Silvestri S, Devetta M, Negro M, Soifer H, Stagira S, Dudovich N, et al. Probe of multielectron dynamics in xenon by caustics in high-order harmonic generation. *Phys Rev Lett*. 2016;117:093902.

15. LaForge AC, Son SK, Mishra D, Ilchen M, Duncanson S, Eronen E, Kukk E, Wirok-Stoletow S, Kolbasova D, Walter P, et al. Resonance-enhanced multiphoton ionization in the x-ray regime. *Phys Rev Lett*. 2021;127:213202.
16. Grobe R, Eberly JH. Observation of coherence transfer by electron-electron correlation. *Phys Rev A*. 1993;48:623–627.
17. Bartschat K, Bray I. Electron-impact ionization of atomic hydrogen from the 1s and 2s states. *J Phys B Atomic Mol Phys*. 1996;29:L577.
18. Bray I, Fursa DV, Kheifets AS, Stelbovics AT. Electrons and photons colliding with atoms: Development and application of the convergent close-coupling method. *J Phys B Atomic Mol Phys*. 2002;35:R117.
19. Colgan J, Pindzola MS, Robicheaux F. Lattice calculations of the photoionization of li. *Phys Rev Lett*. 2004;93:053201.
20. Kheifets AS, Fursa DV, Bray I, Colgan J, Pindzola MS. Differential cross sections of double photoionization of lithium. *Phys Rev A*. 2010;82:023403.
21. Colgan J, Emmanouilidou A, Pindzola MS. Evidence for a T-shape break-up pattern in the triple photoionization of li. *Phys Rev Lett*. 2013;110:063001.
22. Wehlitz R, Huang MT, DePaola BD, Levin JC, Sellin IA, Nagata T, Cooper JW, Azuma Y. Triple photoionization of lithium. *Phys Rev Lett*. 1998;81:1813–1816.
23. Huang M-T, Wehlitz R, Azuma Y, Pibida L, Sellin IA, Cooper JW, Koide M, Ishijima H, Nagata T. Single and double photoionization of lithium. *Phys Rev A*. 1999;59:3397–3401.
24. Zhu G, Schuricke M, Steinmann J, Albrecht J, Ullrich J, Ben-Itzhak I, Zouros TJM, Colgan J, Pindzola MS, Dorn A. Controlling two-electron threshold dynamics in double photoionization of lithium by initial-state preparation. *Phys Rev Lett*. 2009;103:103008.
25. Ruiz C, Plaja L, Roso L. Lithium ionization by a strong laser field. *Phys Rev Lett*. 2005;94:063002.
26. Rapp J, Bauer D. Effects of inner electrons on atomic strong-field-ionization dynamics. *Phys Rev A*. 2014;89:033401.
27. Thiede JH, Eckhardt B, Efimov DK, Prauzner-Bechcicki JS, Zakrzewski J. Ab initio study of time-dependent dynamics in strong-field triple ionization. *Phys Rev A*. 2018;98:031401.
28. Wehlitz R, Bluett JB, Whitfield SB. Comparison of the double- to single-photoionization ratio of li with he. *Phys Rev A*. 2002;66:012701.
29. Kheifets AS, Fursa DV, Bray I. Two-electron photoionization of ground-state lithium. *Phys Rev A*. 2009;80:063413.
30. Kheifets AS, Fursa DV, Hines CW, Bray I, Colgan J, Pindzola MS. Spin effects in double photoionization of lithium. *Phys Rev A*. 2010;81:023418.
31. Efimov DK, Prauzner-Bechcicki JS, Thiede JH, Eckhardt B, Zakrzewski J. Double ionization of a three-electron atom: Spin correlation effects. *Phys Rev A*. 2019;100:063408.
32. Barth I, Smirnova O. Comparison of theory and experiment for nonadiabatic tunneling in circularly polarized fields. *Phys Rev A*. 2013;87:065401.
33. Hartung A, Morales F, Kunitski M, Henrichs K, Laucke A, Richter M, Jahnke T, Kalinin A, Schöffler M, Schmidt LPH, et al. Electron spin polarization in strong-field ionization of xenon atoms. *Nat Photonics*. 2016;10:526–528.
34. Liu M-M, Shao Y, Han M, Ge P, Deng Y, Wu C, Gong Q, Liu Y. Energy- and momentum-resolved photoelectron spin polarization in multiphoton ionization of xe by circularly polarized fields. *Phys Rev Lett*. 2018;120:043201.
35. Trabert D, Hartung A, Eckart S, Trinter F, Kalinin A, Schöffler M, Schmidt LPH, Jahnke T, Kunitski M, Dörner R. Spin and angular momentum in strong-field ionization. *Phys Rev Lett*. 2018;120:043202.
36. Han M, Ge P, Liu M-M, Gong Q, Liu Y. Spatially and temporally controlling electron spin polarization in strong-field ionization using orthogonal two-color laser fields. *Phys Rev A*. 2019;99:023404.
37. Cherepkov N. Spin polarization of atomic and molecular photoelectrons. *Adv At Mol Phys*. 1983;19:395–447.
38. Javanainen J, Eberly JH, Su Q. Numerical simulations of multiphoton ionization and above-threshold electron spectra. *Phys Rev A*. 1988;38:3430–3446.
39. Kosloff R, Kosloff D. Absorbing boundaries for wave propagation problems. *J Comput Phys*. 1986;63:363–376.
40. Crank J, Nicolson P. A practical method for numerical evaluation of solutions of partial differential equations of the heat-conduction type. *Adv Comput Math*. 1947;6:207–226.
41. Li Y, Sato T, Ishikawa KL. High-order harmonic generation enhanced by laser-induced electron recollision. *Phys Rev A*. 2019;99:043401.
42. Sainadh US, Xu H, Wang X, Atia-Tul-Noor A, Wallace WC, Douguet N, Bray A, Ivanov I, Bartschat K, Kheifets A, et al. Attosecond angular streaking and tunnelling time in atomic hydrogen. *Nature*. 2019;568:75–77.
43. Pazourek R, Nagele S, Burgdörfer J. Probing time-ordering in two-photon double ionization of helium on the attosecond time scale. *J Phys B Atomic Mol Phys*. 2015;48:061002.
44. Baum G, Blask W, Freienstein P, Frost L, Hesse S, Raith W, Rappolt P, Streun M. Spin asymmetries for triple-differential electron-impact ionization of lithium at 54.4 ev. *Phys Rev Lett*. 1992;69:3037–3040.
45. Streun M, Baum G, Blask W, Berakdar J. Role of exchange and kinematic in the generation of low-energy polarized electron pairs. *Phys Rev A*. 1999;59:R4109–R4112.
46. Kang H-S, Ko IS. Attosecond xfel for pump-probe experiments. *Nat Photonics*. 2019;14:7–8.